Polymer 51 (2010) 5612–5622

Contents lists available at ScienceDirect

Polymer

journal homepage: www.elsevier.com/locate/polymer

A polyethylene chain investigated with replica exchange molecular dynamics simulation: Equilibrium lamellar thickness and melting point, ordering and free energy

Ting Li [a,b,**], Zhouting Jiang [c,d], Dadong Yan [e], Erik Nies [a,d,*]

[a] Polymer Research Division, Department of Chemistry and The Leuven Mathematical Modeling and Computational Science Centre (LMCC), Katholieke Universiteit Leuven, Celestijnenlaan 200F, B-3001 Heverlee, Belgium
[b] State Key Laboratory of Polymer Physics & Chemistry, Center for Molecular Science, Institute of Chemistry, Chinese Academy of Sciences, Zhongguancun, Beijing 100080, Peoples' Republic of China
[c] Department of Applied Physics, China Jiliang University, Hangzhou 310018, China
[d] Laboratory of Polymer Technology, Eindhoven University of Technology, P.O. Box 513, 5600MB Eindhoven, The Netherlands
[e] Department of Physics, Beijing Normal University, Beijing 100875, China

ARTICLE INFO

Article history:
Received 8 July 2010
Received in revised form
8 September 2010
Accepted 8 September 2010
Available online 17 September 2010

Keywords:
Coil-globule-folded chain transition
Free energy
Replica exchange molecular dynamics

ABSTRACT

In the present work, a polyethylene chain with $N = 200$ *CH*2 units was simulated using replica exchange molecular dynamics (REMD). Simulations were performed in a broad temperature range and for intra-chain interactions varying from the fully interacting to the ideal spring chain.

Our work demonstrates that REMD is a very efficient method to obtain equilibrium data. It is found that the coil-to-globule transition is dominated by the vdW energy, whereas the globule-to-folded chain transition is accompanied by transitional behavior in the torsion and vdW energies. Our data clearly show that for the chain length considered here, the chain folded crystal to globule transition is a continuous transition. Nevertheless, we can establish with good accuracy the equilibrium transition temperature for the chain folded crystal to globule transition.

A set of orientational order parameters was used to investigate the order in the polymer chain. At the globule-to-folded chain transition an abrupt change in the value of the order parameter is observed, whereas there is no or almost no change in the value of the order parameter at the coil-to-globule transition temperature. The (apparent) order in the disordered globular and coiled states indicated by some studied order parameters is related to the definition of the order parameter and depends on the chain length of the polymer.

Below the equilibrium melting temperature the (largest principal component of the) radius of gyration and the equilibrium lamellar thickness of the folded chain crystal decrease with increasing temperature, which gives support to the theory of Muthukumar but is opposite to the prediction of classical crystallization theories. The agreement between simulations and theory may hint to universal behavior of the relative equilibrium thickness versus the relative super cooling.

1. Introduction

For many decades the properties of the single polymer chain have been actively studied by experiment [1–18], theory [19–23] and simulation [24–39]. The single chain behavior is elementary to understand the properties of polymers in the condensed state (pure as well as in mixtures and solutions) but the single chain has also immediate relevance in nano-sciene, nano-technology and experimental techniques, such as AFM, which allows for the direct study of single chains. Swislow et al. [40] were the first to experimentally observe in dilute solution below the Θ-temperature the

* Corresponding author. Polymer Research Division, Department of Chemistry and The Leuven Mathematical Modeling and Computational Science Centre (LMCC), Katholieke Universiteit Leuven, Celestijnenlaan 200F, B-3001 Heverlee, Belgium. Tel.: +32 16 327481/418; fax: +32 16 327990.
** Corresponding author. Polymer Research Division, Department of Chemistry and The Leuven Mathematical Modeling and Computational Science Centre (LMCC), Katholieke Universiteit Leuven, Celestijnenlaan 200F, B-3001 Heverlee, Belgium. Tel.: +32 16 327614; fax: +32 16 327990.
E-mail addresses: Ting.Li@chem.kuleuven.be (T. Li), E.L.F.Nies@tue.nl (E. Nies).

0032-3861/$ – see front matter © 2010 Elsevier Ltd. All rights reserved.
doi:10.1016/j.polymer.2010.09.019

collapse from the expanded coil to the dense globule of isolated atactic polystyrene chains. However, the expanded coil and the globular state are not the only possible chain conformational states and depending on the details of the intra-chain and chain–solvent interactions other conformational states may exist for non-crystallisable polymer chains [30,41–43].

From the simulation and theoretical points of view the existence of different single chain conformational states and transitions between them has been studied in quite some detail [24,44]. For instance, the occurrence of the globular state upon going from the expanded coil to the chain folded chain crystal and the length/diameter aspect ratio of the chain folded single molecule crystal sensitively depends on the chain stiffness [41,45,46] and the chain length [44].

Also the dynamic process of chain folding upon cooling or heating, the subsequent rearrangement and melting of the chain folded crystal have been investigated intensively by computer simulation. For example, it has been observed [47] that the melting behavior of the single chain folded crystal depends on the heating conditions. This can be seen as a consequence of the very rugged free energy landscape of the single chain at the low temperatures where the chain folded states are preferred. This also brings to attention one of the problems with some molecular simulation techniques: different chain folded conformational states are very likely separated by high free energy barriers, making it very difficult to realize transitions from one state to the other in the time of a single Molecular Dynamics or conventional Monte Carlo simulation run. As a consequence the simulation does not necessarily represent a proper ensemble average overall relevant chain conformational states. Therefore, the simulation results are not necessarily representative of the behavior of real chains observed in typical experiments, in which the time of the experiment is sufficiently long and/or the number of chains probed by the experiment is sufficiently large to sample the different conformational states much easier. To overcome the problem of poor sampling of the rugged free energy landscape, advanced simulation methods have been developed. In particular expanded ensemble simulation methods, such as the replica exchange (REM) or parallel tempering (PT) [48–51], multicanonical ensemble method (MUCA) [52–54] and four dimensional expanded ensemble algorithm [55,56], have proven to be very efficient.

In this work we apply for a polyethylene chain of finite length (200 *CH2* units) canonical MD simulations combined with the replica exchange molecular dynamics (REMD) [57–59] to explore a wide range of temperatures and variations in intra-chain interactions enabling us to efficiently sample the whole relevant phase space and to provide simulation data of high quality which are representative for the equilibrium behavior of the chain molecule; also at the lowest investigated temperatures. Using the simulation data we perform a set of thermodynamic integrations to determine the absolute free energy, entropy and internal energy of the single chain as a function of temperature. Our data allow for a detailed analysis of the thermodynamics, the conformational properties and ordering of the chain in the encountered conformational states. Finally, our data also allow us to test a recent theoretical development considering the chain crystallization and melting from a thermodynamic equilibrium perspective.

The paper is organized as follows. First the model and simulation parameters are described. Then, the simulation results of the thermodynamic and structural analysis are presented and finally the data are used to make contact with the recent theory of Muthukumar on chain crystallization and melting emphasizing the importance of the chain folds in determining the equilibrium behavior of the chain folded crystal. Finally, some conclusions are made.

2. Simulation details

In this study, a linear polyethylene chain with chain length $N = 200$ *CH2* groups was modeled as a bead-spring chain using the united atom (UA) approximation for the *CH2* units and making no distinction between middle and end groups. The united atom approximation is widely used in the simulation of macromolecules [25,60–62]. Four types of potentials are included in our simulation, i.e. bond stretching, angle bending, torsional rotation and van der Waals (vdW) interactions between atoms separated more than two covalent bonds along the polymer chain (i.e. including the 1–4 interaction). The potential energy expressions and the parameter values for the united atom model are taken from the DREIGING force field [63]:

$$U = U_{\text{bond}} + U_{\text{angle}} + U_{\text{torsion}} + U_{\text{vdW}}, \tag{1}$$

in which, $U_{\text{bond}} = \sum \frac{1}{2} K_b (l - l_0)^2$, $U_{\text{angle}} = \sum \frac{1}{2} K_a (\theta - \theta_0)^2$ $U_{\text{torsion}} = \sum \frac{1}{2} K_t \{1 - \cos[n(\varphi - \varphi_0)]\}$ and $U_{\text{vdW}} = \sum\sum 4\varepsilon[(\frac{\sigma}{r})^{12} - (\frac{\sigma}{r})^6]$ (The summation denotes that the potential energy terms are summation for all bonds, angles, torsion angles and non-bonded pairs respectively.) and parameter values are given in Table S1 of the Supplementary information.

In the following we use reduced units. The van der Waals diameter σ, the energy parameter ε and the mass of the united atom are taken to define reduced units that are denoted by the superscript asterisk, for example, $T^* = k_B T/\varepsilon$, $\rho^* = \rho\sigma^3$, $t^* = t\sqrt{\varepsilon/m}/\sigma$, $r^* = r/\sigma$, $v^* = v\sqrt{m/\varepsilon}$ and $C_v^* = C_v/k_B$. For the particular parameter values used in this study (see Supplementary information, Table S1) the following conversions are obtained: $t = 1.488 \times t^*$ with the time t in picosecond, and $T = 99.921 \times T^*$ with the temperature T in Kelvin. In the constant temperature REMD simulations massive Nose-Hoover chain (MNHC) thermostat [64] was employed and the reduced time step was $\Delta t^* = 1.6427 \times 10^{-3}$ (or 2.444 femtosecond in real units).

A REMD or parallel tempering molecular dynamics (PTMD) simulation with in total 77 temperatures, covering a wide temperature range from 252 K to 1511 K, was executed. The set of reduced temperature values are given in Table S2 of the Supplementary information.

In a second REMD run the following λ-dependent potential was used

$$U_\lambda(\lambda) = U_{\text{bond}} + U_{\text{angle}}(\lambda) + U_{\text{torsion}}(\lambda) + U_{\text{vdW}}(\lambda), \tag{2}$$

in which $U_{\text{bond}} = \sum \frac{1}{2} K_b (l - l_0)^2$ as in equation (1), $U_{\text{angle}}(\lambda) = \sum \frac{1}{2} \lambda K_a (\theta - \theta_0)^2$, $U_{\text{torsion}}(\lambda) = \sum \frac{1}{2} \lambda K_t \{1 - \cos[n(\varphi - \varphi_0)]\}$ and $U_{\text{vdW}}(\lambda) = \sum\sum 4\varepsilon[(\frac{\lambda\sigma}{r})^{12} - (\frac{\lambda\sigma}{r})^6]$

When $\lambda = 1$, $U_\lambda(\lambda)$ is the same as in the original force field. When $\lambda = 0$, U_{bond} is the only energy contribution representing the ideal spring chain.

The second REMD simulation was run with in total 29 λ values in the interval $0 \leq \lambda \leq 1$, which are also provided in Table S3 the supplementary information.

3. Results and discussion

3.1. Thermodynamics-heat capacity, potential energy probability density distribution and absolute free energy

3.1.1. Heat capacities

It is straightforward to calculate the isothermal heat capacity at constant volume from the simulation data. In Fig. 1. the isothermal heat capacities are shown for the total energy (kinetic plus potential), the total potential energy, and the different

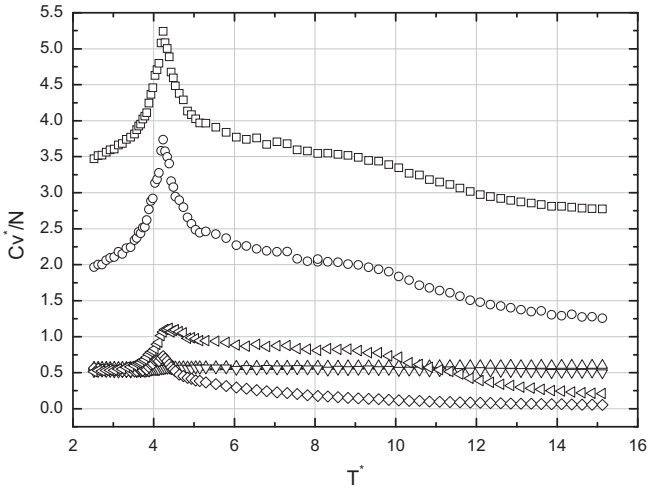

Fig. 1. Reduced specific total heat capacity (squares) and the contributions from the total potential energy (circles), the bond (upward triangles), angle bending (downward triangles), torsion (diamonds) and vdW (leftward triangles) energies as functions of temperature.

contributions to the potential energy (vdW, bonding, angle and torsion potential energies) and are calculated from

$$C^*_{V,\text{total}} = \frac{\left\langle H^{*2}\right\rangle - \left\langle H^*\right\rangle^2}{\left\langle T^*\right\rangle^2} \tag{3a}$$

$$C^*_{V,\text{potential}} = \frac{\left\langle U^{*2}\right\rangle - \left\langle U^*\right\rangle^2}{\left\langle T^*\right\rangle^2} \tag{3b}$$

$$C^*_{\text{V,vdW}} = \frac{\left\langle U^{*2}_{\text{vdW}}\right\rangle - \left\langle U^*_{\text{vdW}}\right\rangle^2}{\left\langle T^*\right\rangle^2} \tag{3c}$$

$$C^*_{\text{V,bond}} = \frac{\left\langle U^{*2}_{\text{bond}}\right\rangle - \left\langle U^*_{\text{bond}}\right\rangle^2}{\left\langle T^*\right\rangle^2} \tag{3d}$$

$$C^*_{\text{V,angle}} = \frac{\left\langle U^{*2}_{\text{angle}}\right\rangle - \left\langle U^*_{\text{angle}}\right\rangle^2}{\left\langle T^*\right\rangle^2} \tag{3e}$$

$$C^*_{\text{V,torsion}} = \frac{\left\langle U^{*2}_{\text{torsion}}\right\rangle - \left\langle U^*_{\text{torsion}}\right\rangle^2}{\left\langle T^*\right\rangle^2} \tag{3f}$$

with $H^* = U^* + K^*$, the Hamiltonian and K^* the kinetic energy of the system in reduced units.

As we can see the difference between the total heat capacity (from kinetic and potential energy) and the heat capacity derived from the total potential energy is within simulation uncertainty 1.5 at all temperatures in agreement with the equipartition theorem. This is also a proof that our simulation was very well equilibrated in momentum space, providing evidence of the correct and efficient working of the MNHC thermostat.

The heat capacities calculated from the bonding and angle energy fluctuations are constant at all temperatures, indicating that these degrees of freedom are not responsible for the transition behavior seen in the total heat capacity. In this respect, the contributions from the van der Waals interaction and the torsion conformational energy are the most interesting.

At very low temperatures, the *CH2* segments are practically fixed to the lattice positions of the crystal lattice and only local vibrations and position adjustments are allowed. This is reflected by $C^*_{\text{V,vdW}}$, which is flat in Fig. 1. when $T^* < 3.53$. As the temperature increases, $C^*_{\text{V,vdW}}$, $C^*_{\text{V,torsion}}$ and $C^*_{\text{V,total}}$ have a sharp peak at $T^* \cong 4.23$ clearly indicating the occurrence of a transition (i.e. the chain folded lamellar crystal to globule transition to be discussed in more detail below). At the transition temperature the polymer chain experiences substantial fluctuations in the torsion energy. At the same time, the vdW energy is also fluctuating in order to re-arrange the *CH2* segments from the regular crystalline configuration into a more liquid like organization in the globular state. From the transition temperature $T^* \cong 4.23$ all C_Vs decrease with increasing temperature. A shoulder peak in $C^*_{\text{V,vdW}}$ and $C^*_{\text{V,total}}$ but not in $C^*_{\text{V,torsion}}$ can be observed at the coil-to-globule transition temperature (to be discussed below in relationship to the temperature dependence of the radius of gyration of the chain), indicating that the coil-to-globule transition is mainly caused by the van der Waals interaction and has little to do with the local chain conformation. In fact, the observation is very similar to the collapse transition observed in Lennard-Jones clusters [65].

3.1.2. Potential energy probability density distributions

In Fig. 2 the potential energy probability density distribution functions of the 77 different temperatures are presented. It can be seen that at each temperature the potential energy probability density distribution curve has a smooth Gaussian shape. This indicates that in the parallel tempering simulation we have achieved efficient and sufficient sampling of the phase space also at the lowest temperatures, which is not realized in a conventional simulation. The distribution curve in red (shown separately in the inset of Fig. 2.) is at the temperature $T^* \cong 4.23$ where the potential energy probability density distribution height reaches a local minimum. At this temperature also a transition was observed in several of the heat capacities. Below this temperature, the heights of the probability density distributions increase almost linearly with decreasing temperature. For higher temperatures, i.e. $T^* > 4.23$, the height of the energy probability densities increase until a maximum at $T^* = 4.64$ and then monotonically decreases to high temperature.

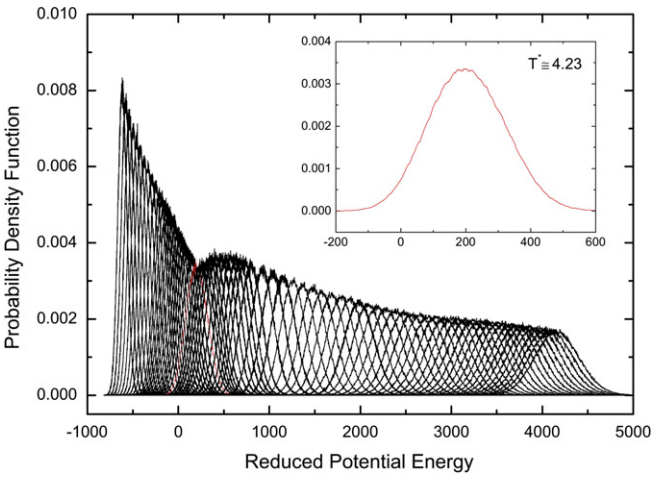

Fig. 2. Potential energy probability density functions of the 77 canonical ensemble (NVT) replicas in our REMD simulation. The distribution shifts right (higher energy) with increasing temperature. The inset shows the PDF at the melting point $T^* \cong 4.23$. No bimodality can be seen in the distributions.

It is important to note that at $T^* \cong 4.23$ or any other temperature we do not observe a bimodal energy probability density distribution, indicative of the coexistence of two states as in a first order phase transition. This may come as a surprise; however, the presence or absence of a bimodal energy probability density distribution may depend sensitively on the specific interaction model used and on the chain length. For example, it was shown that variations in the strength of the bending potential in a bead-stick chain model with angle bending and square-well non-bonded interactions, a bimodal potential energy distribution changed from bimodal to unimodal [30]. In a similar manner a freely jointed square-well chain with a tunable width of the non-bonded square-well potential bimodal potential energy distributions were observed for chains of 32mer and 64mer, which could clearly be interpreted in terms of a first order transition. However, reducing the width of the square-well to a slightly smaller value, the energy distribution of the 64mer changed from bimodal to unimodal. The authors concluded that the range of the attraction is crucial for the bimodality of the potential energy distribution and the strength of the first order transition to a solid in a finite system [65]. Effects of the potential function parameters have been observed also in systematic studies in the crystallization and melting transition of polymer melts. Using a carefully tuned coarse grained potential model Meyer et al. studied the crystallization and melting behavior of polymer melts as a function of chain length and parameter values in the coarse grained potential model [66–68]. For example it was shown that the angular interaction in the coarse grained potential model on the crystallization and melting behavior influences the volume change upon cooling and heating at the transition temperature (T_c and T_m). With increasing flexibility the volume changes at the transition temperatures were observed to diminish and to become more gradual [67,68]. When the angular potential was removed completely the system did not crystallize but vitrified [66]. These all may be indications that the transitional behavior is changing from clear first order to a more continuous transition.

3.1.3. Average potential and total energy, absolute free energy, absolute entropy and absolute energy

Fig. 3 shows the average potential energy and total energy (potential plus kinetic) as a function of temperature. Also here a rounded but recognizable step is found around the transition temperature ($T^* \cong 4.23$).

The parallel tempering MD simulation run can be used to get the free energy difference of the real interacting chain at temperatures T and T_0 from the following thermodynamic integration

$$\Delta A_1^*\left(T^*\right) = \frac{A^*\left(T^*\right)}{T^*} - \frac{A^*\left(T_0^*\right)}{T_0^*} = \int_{\frac{1}{T_0^*}}^{\frac{1}{T^*}} \left\langle U^*\left(T^{*\text{“}}\right)\right\rangle d\left(\frac{1}{T^{*\text{”}}}\right) \tag{4a}$$

and

$$A^*\left(T^*\right) = \frac{T^*}{T_0^*}A^*\left(T_0^*\right) + T^*\Delta A_1^*\left(T^*, T_0^*\right) \tag{4b}$$

where $A^*(T)$ and $U^*(T^*)$ are the reduced Helmholtz free energy and total energy of the system at temperature T^* respectively. The angular brackets in equation (4a) indicate as before the ensemble average.$\langle U^*(T^*)\rangle$ is obtained directly from the results of the REMD simulation, which has been presented in Fig. 3. T_0^* is a reference temperature which we have chosen here to be the highest temperature 15.121 in reduced unit. The free energy change $\Delta A_1^*(T^*, T_0^*)$ calculated by this integration, equation (4a), is shown in Fig. 4.

Moreover, by choosing an appropriate reference state one can further calculate the *absolute free energy* of the fully interacting chain. In the following we calculate from another REMD simulation at the reference temperature T_0^* the free energy difference between the fully interacting chain and the ideal spring chain, defined in the *Section Simulation details*. In this second parallel tempering simulation, the strengths of the angular and torsion potentials as well as the diameter σ in the Lennard-Jones potential are changed gradually from zero to the actual values defined in the force field. The free energy difference between the ideal spring chain and the fully interacting PE chain is then determined at the chosen reference temperature T_0^* from the following λ-integration.

$$\begin{aligned}\Delta A_2^*\left(\lambda, T_0^*\right) &= A^*\left(\lambda, T_0^*\right) - A^*_{\text{ideal spring chain}}\left(T_0^*\right) \\ &= \int_0^{\lambda} \left\langle \frac{dU^*\left(\lambda^{\text{“}}\right)}{d\lambda^{\text{”}}} \right\rangle d\lambda^{\text{“}}\end{aligned} \tag{5a}$$

and

$$A^*\left(\lambda, T_0^*\right) = A^*_{\text{ideal spring chain}}\left(T_0^*\right) = \Delta A_2^*\left(\lambda, T_0^*\right) \tag{5b}$$

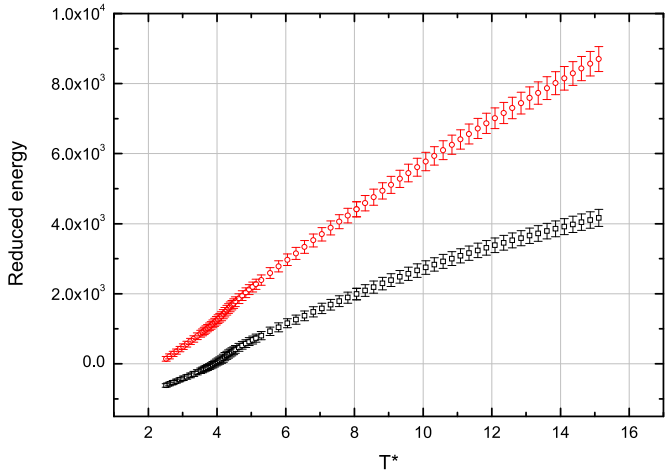

Fig. 3. The total energy (circles) and potential energy (squares) of the PE model chain as a function of temperature.

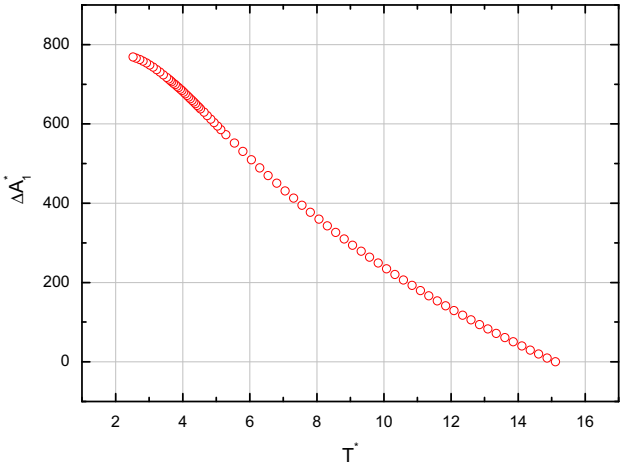

Fig. 4. The free energy difference ΔA_1^* of the PE model chain at different temperatures with respect to the free energy at the highest temperature $T_0^* = 15.121$

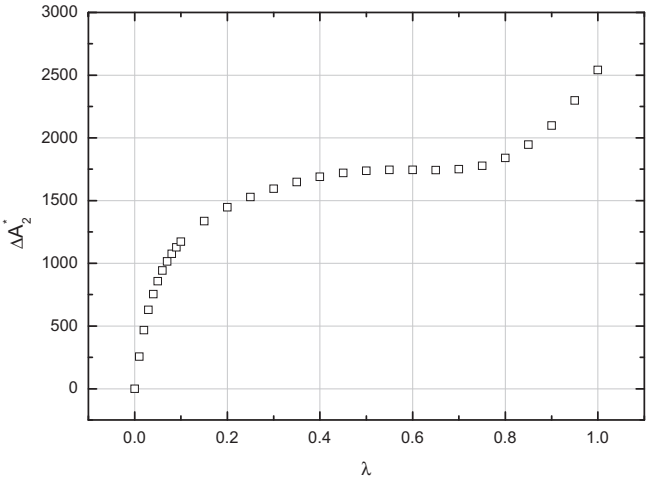

Fig. 5. The free energy difference $\Delta A_2^*(\lambda, T_0^*)$ between the ideal spring chain and the chain with $U^*(\lambda)$ as a function of λ.

The free energy difference between the ideal spring chain and the chain with $U^*(\lambda)$ is presented as a function of λ in Fig. 5.

At $\lambda = 1$ the fully interacting chains is recovered and the difference in free energy between the ideal spring and the real chain can be determined. The free energy difference between the real chain and the ideal spring chain is found to be $\Delta A_2^*(\lambda = 1, T_0^*) = 2541.119$.

Finally, the free energy of the ideal spring chain $A^*_{\text{ideal spring chain}}(T_0^*)$ can be calculated analytically. The details of this are given in the Supplementary Information. For the PE chain used in our simulations, $N = 200$, $k_{\text{bond}} = 700$ $kcal \cdot mol^{-1}$ Å^{-2}, $l_0 = 1.53\text{Å}$ and $A^*_{\text{ideal spring chain}}(T_0^*) = 249.092$.

The reduced *absolute free energy* of the real PE chain as a function of temperature (see equation (6)) presented in Fig. 6 is obtained from the combination of $A^*_{\text{ideal spring chain}}(T_0^*)$, $\Delta A_2^*(\lambda, T_0^*)$ and $\Delta A_1^*(T^*, T_0^*)$ according to

$$A^*(T) = \frac{T^*}{T_0^*}\left(A^*_{\text{ideal spring chain}}\left(T_0^*\right) + \Delta A_2^*\left(\lambda = 1, T_0^*\right)\right) + T^* \Delta A_1^*\left(T^*, T_0^*\right) \quad (6)$$

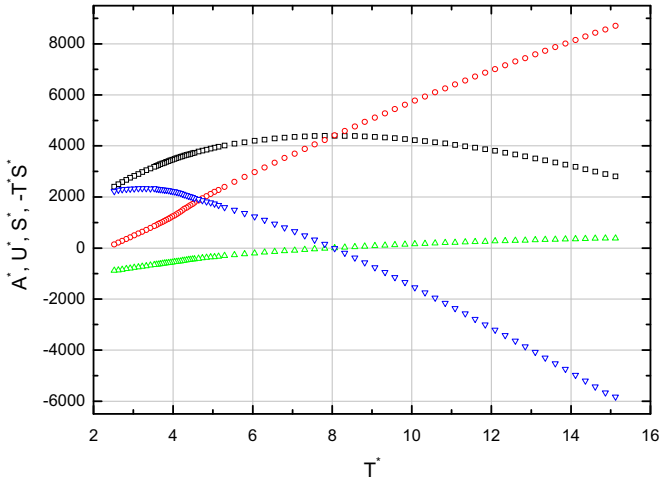

Fig. 6. The absolute free energy (squares), internal energy (circles), entropy (upward triangles) as functions of the reduced temperature. The negative of the product of temperature and entropy (downward triangles) is also presented for the convenience of checking the contribution to the total free energy.

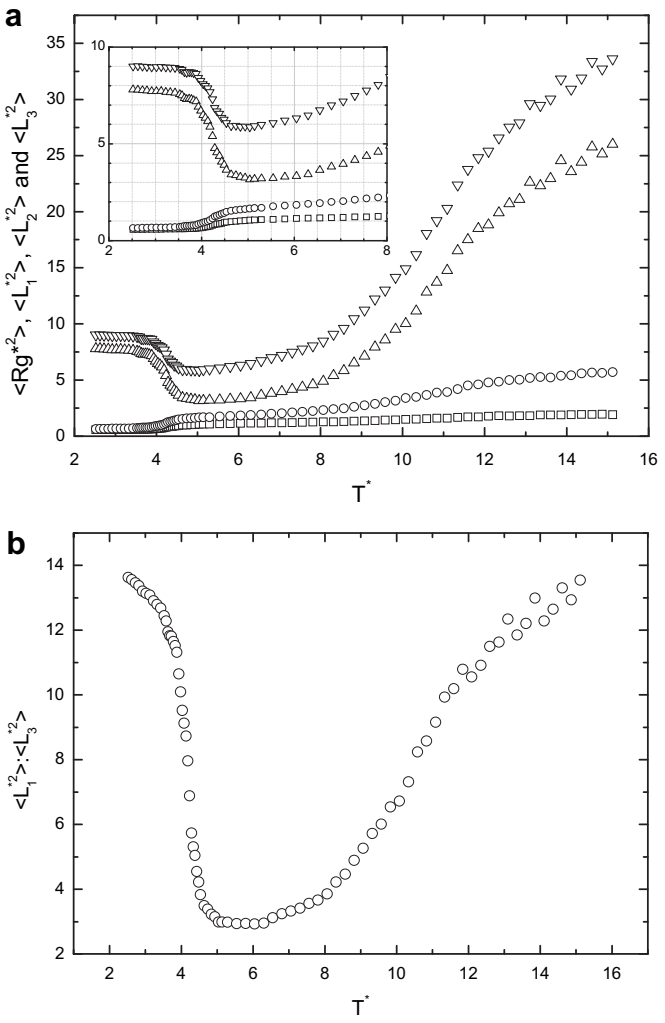

Fig. 7. (a) Mean squared radius of gyration $\langle Rg^{*2}\rangle$ (downward triangles) and its principal components $\langle L_1^{*2}\rangle$ (upward triangles, the largest component), $\langle L_2^{*2}\rangle$ (circles) and $\langle L_3^{*2}\rangle$ (squares, the smallest component) as functions of temperature. The inset presents an enlarged view of the lower temperature region. (b) The ratio between $\langle L_1^{*2}\rangle$ and $\langle L_3^{*2}\rangle$ as a function of temperature.

In addition, the entropy and the internal energy of the PE chain can be calculated from $S^*(T^*) = -\frac{dA^*(T^*)}{dT^*}$ and $E^*(T^*) = A^*(T^*) + T^*S^*(T^*)$. The reduced entropy and reduced energy of the real PE chain as a function of temperature are presented in Fig. 6. Note that the reduced energy obtained in this way is, as it should be, in quantitative agreement with the total energy directly obtained from the simulations, proving the correctness and internal consistency of our calculations.

We can see that both the internal energy and entropy increases monotonically with increasing temperature and there is an obvious maximum in the free energy. Similar features for internal energy and entropy are also seen in the work of Rampf *et al.*, [44] where the free energy and entropy of a bond fluctuation model (BFM) chain with square-well interactions with a similar length are presented as functions of temperature. In many studies, single chain folding is addressed as first order phase transition. However, for the PE chain model studied here only smoothed stepwise changes are seen in the entropy and the internal energy at the transition temperature $T^* \cong 4.23$ and in the free energy a discrete change in slope is not observed at the transition temperature.

3.2. Radius of gyration

The radius of gyration *Rg* is a basic measure of the overall size of a chain molecule. To get insight in the average shape of a chain molecule *Rg* is usually decomposed into the three components along the principal axes of the moment of inertia of the polymer chain, which are denoted as L_1, L_2 and L_3 with L_1 the largest component and L_3 the smallest one [69]. In Fig. 7(a), the reduced mean squared radius of gyration $\langle Rg^{*2}\rangle$ and its three principal components $\langle L_1^{*2}\rangle$, $\langle L_1^{*2}\rangle$ and $\langle L_3^{*2}\rangle$ are shown as functions of reduced temperature.

In Fig. 7(a) two transitions can be clearly seen in the whole temperature range. The one at higher temperature ($T^* = 10.83$) represents the coil-to-globule transition. Above this temperature the chain exists in an expanded coil state characterized by a high ratio of $\langle L_1^{*2}\rangle : \langle L_3^{*2}\rangle$ (See Fig. 7(b).). This indicates the chain has a highly non-spherical instantaneous shape in this regime. As the temperature decreases below the coil-to-globule transition temperature, the polymer chain collapses into a compact globule. The ratio of $\langle L_1^{*2}\rangle : \langle L_3^{*2}\rangle$ decreases substantially, indicating that the chain shape becomes more spherical although $\langle L_1^{*2}\rangle : \langle L_3^{*2}\rangle$ will never go exactly to 1. The coil-to-globule transition is caused by the attractive van der Waals interactions and the tendency to make a more spherical globule can be seen as a consequence of the chain to minimize its surface free energy at higher globular segmental number density [70].

As the temperature decreases, the overall mean squared radius of gyration $\langle Rg^{*2}\rangle$ reaches a minimum at $T^* \cong 5.04$ indicating the chain contracts into a very condense globule. After reaching its minimal size in $\langle Rg^{*2}\rangle$ the chain shows a new quite sharp increase at $T^* \cong 4.23$, which can be attributed to the crystallization of the single chain. In this low temperature regime the polymer chain transforms from the condensed globule to a chain folded lamellar state, in which the chain folds back and forth and the stems of chain segments in the *all trans*- conformation arrange parallel with each other. In Fig. 7(a) we see that $\langle L_1^{*2}\rangle$ increases while $\langle L_2^{*2}\rangle$ and $\langle L_3^{*2}\rangle$ decrease, which indicates that the folded chain lamella has an overall rod-like shape, with $\langle L_1^{*2}\rangle$ that can be seen as a measure of the squared thickness of the lamella, i.e. the squared fold length of the lamellar crystal. As the temperature continues to decrease, $T^* < 4.0$, in Fig. 7(a) we see a small but systematic increase of $\langle L_1^{*2}\rangle$ and decrease of $\langle L_2^{*2}\rangle$ and $\langle L_3^{*2}\rangle$ indicating that the lamellar fold length increases with decreasing temperature.

The observation of chain folding of the single PE chain in simulations is not new and is well documented, dating back to the original work of Kavassalis and Sundararajan using conventional MD simulations [71]. Following these authors many single chain simulations have been reported, studying the single chain behavior under various conditions. For instance, Fujiwara et al. [72] observed in a conventional MD simulation of a single chain molecule that upon quenching the chain from high temperature well above the equilibrium melting temperature T_m^0 to several low temperatures chain folding occurs. Lamellar thickening is observed with reduced quenching depth. Similar behavior was also observed by Liu and Muthukumar [73] Zhang et al. [74] found, using the same force field as in the present work, that a folded PE chain, well equilibrated at a particular crystallization temperature, also thickened upon heating to a temperature closer to T_m^0. These findings were interpreted to be in agreement with the results of classical kinetic crystallization theory which predicts that the lamellar thickness of a chain folded crystal is inversely proportional to the super cooling $\Delta T = T_m^0 - T_c$ and that lamellar thickening should occur upon heating the chain folded crystal.

In stark contrast with these studies of the kinetic process, we observe a decrease in lamellar fold length upon approaching the equilibrium melting temperature of the chain folded crystal. We should emphasize that in our REMD simulations we obtain thermodynamic equilibrium data and hence the observed lamellar thickness represents the equilibrium thickness of the chain folded crystal which is (virtually) impossible to obtain in a conventional MD simulation as the chain will be trapped in a chain folded structure that is merely one possible realization of the chain folded crystal. In our REMD simulations we get a significantly improved sampling of the whole relevant phase space and thus obtaining more accurate information on the equilibrium chain folded crystal thickness.

3.3. Orientational order parameters

3.3.1. Order parameters

To quantify the ordering in the folded chain structures different orientational order parameters have already been used [75]. A first choice to define an order parameter is to build the ordering tensor [76,77].

$$S_{ij} = \frac{1}{2}(3u_i u_j - \delta_{ij}) \tag{7}$$

where u_i and u_j are unit vectors defining the directions of the *all trans* stems, $u_i u_j$ denotes the dyadic tensor product, δ_{ij} denotes the Kronecker delta and $\langle\cdots\rangle$ denotes the usual thermodynamic ensemble average overall the *all-trans* stem pairs. More specifically, in an *all-trans* stem, all the torsion angles formed by at least four consecutive chain units fall in the angular ranges $[-\pi, -5\pi/6)$ or $(5\pi/6, \pi]$. Then the two united atoms at the two ends of the *all-trans* stem are used to define the vector u_i. S_{ij} is a 3×3 tensor matrix in a 3D Cartesian coordinate system. By diagonalizing S_{ij}, three eigenvalues λ_1, λ_2 and λ_3 are obtained, which can be used directly as measure of the ordering of *all-trans* stems. The largest eigenvalue λ_1 provides information on the orientational order along direction of its eigenvector n and the two eigenvalues, λ_2 and λ_3 provide information on the orientational order in the two mutually perpendicular directions at right angles to n.

Another method to define order parameters makes use of the second Legendre polynomial

$$\langle P_2(\cos\theta)\rangle = \left\langle \frac{3\cos^2\theta - 1}{2} \right\rangle \tag{8}$$

where θ is the angle between a preferred director $\boldsymbol{n}$ and e.g. the bond or stem vectors.

For instance, we can use the eigenvector $\boldsymbol{n}$ associated with the largest eigenvalue λ_1 as the director in equation (7) and define an order parameter, denoted by OP_2 [76].

Finally, OP_3 is the order parameter calculated by equation (7) with the director $\boldsymbol{n}$ the eigenvector associated with the principal axis associated with L_1, the largest principal component of the radius of gyration. OP_3 has been used by Fujiwara and Sato to study the bond orientational order [78].

For notational convenience we will denote the eigenvalue λ_1 also by OP_1 [77]. The definitions of all order parameters used in this work are summarized in Table 1.

Fig. 8 shows the eigenvalues λ_1, $-\lambda_2$ and $-\lambda_3$ as a function of temperature. A clear transition exists at $T^* \cong 4.23$, the same temperature at which the compact globule transforms into a chain folded lamella in Fig. 7(a) and (b) and the transition temperature determined in the thermodynamic properties i.e. the energy probability density distribution $P(U)$, the heat capacities and the absolute internal energy and entropy.

The increase of λ_1 denotes that the ordering of the polymer chain occurs within a very narrow temperature range. Unlike the behavior

Table 1
Summary of the order parameters used in this work.

Order parameter	definition	comment
$OP_1 \equiv \lambda_1$	The largest eigenvalue of the ordering tensor defined by Eq. (7)	Without using any predefined director.
λ_2,λ_3	The second largest and the smallest eigenvalues of the ordering tensor defined by Eq. (7)	Without using any predefined director.
OP_2	The order parameter defined by Eq. (8) by taking the eigenvector of λ_1 as the director	Using predefined director
OP_3	The order parameter defined by Eq. (8) by taking the principal axis associated with L_1 (the largest principal component of radius of gyration) as the director	Using predefined director

of the radius of gyration and its principal components presented in Fig. 7(a), the order parameter shows no abrupt changes at the coil-to-globule transition temperature, demonstrating that the orientational ordering in the globule and coiled state are both low although a systematical increase of the number of trans- torsional angles can be observed while lowering the temperature as we shall see in Fig. 8.

In Fig. 8 it can be observed that all the order parameters λ_1, λ_2 and λ_3 remain at a non-zero value even at high temperatures; which can be seen as a consequence of the finite size of the chain molecule [77,79]. It has been shown that in the limit of complete disorder (high temperature) λ_1, and λ_3 will asymptotically approach the same value, proportional to $1/N^{0.5}$ and λ_2 will attain a smaller value; proportional to $1/N$ with N the number of particles or segments in the chain. In the ordered state one should approximately get $\lambda_3 \approx -\lambda_1/2 - c$ and $\lambda_2 \approx -\lambda_1/2 + c$ with $c \sim 1/N^{0.5}$ a positive number, which gives $\lambda_1 > |\lambda_3| > |\lambda_2|$ [77]. In Fig. 8 it can be seen that these inequalities are met by our data.

In Fig. 9(a) we compare the results for the order parameter definitions ($OP_1 \equiv \lambda_1$, OP_2, and OP_3) used in previous studies. All order parameters give the same transition temperature for the globule-to-chain folded lamella transformation. This is clarified in Fig. 9(b), where the first order derivatives of the order parameters are shown. This indicates all of them could be used as indicators of ordering in the study of chain folding.

However, differences among these order parameters can be seen in Fig. 9(a). As already noted in Fig. 8 $OP_1 \equiv \lambda_1$ does not go to zero at high temperature, the same applies to OP_3 which asymptotically seems to go to a small but non-zero value at high temperature. On the other hand the simulation data seem to indicate that, despite the finite size of the chain, the order parameter OP_2 approaches zero asymptotically, as can be inferred from the logarithmic presentation used in Fig. 8. This makes OP_2 a convenient order parameter to quantify order and disorder in the chain molecule. The behavior of the widely used definition OP_3 deserves a further remark.

At the low temperature end, OP_3 has similar absolute values as OP_1. However, OP_3 shows a gradual increase of the order in the coil and globule regimes ($5.04 < T^* < 10.08$) with decreasing temperature. Thus from OP_3 it could be concluded that the order in the globule is significant and changes continuously. This is in contrast with the order parameter definitions which do not vary significantly in the coiled and globular states and only show more ordering for temperatures much closer to the transition temperature. Thus the use of OP_3 may lead to wrong conclusions about the order in the globular state. The difference is related in this case to the choice of the preferred director $\boldsymbol{n}$. In OP_3 we use the direction of the largest principal component of the radius of gyration of the chain molecule. In the instantaneous shape we have a preferred orientation of the chain segments along the director.

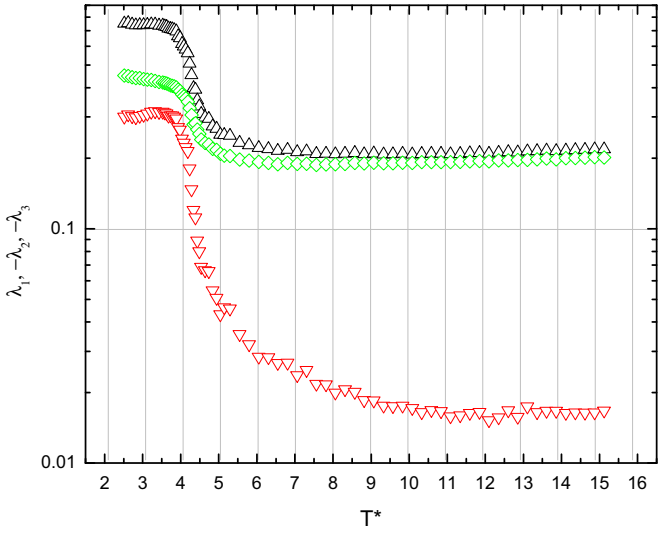

Fig. 8. Eigenvalues of the order parameter tensor matrix defined by Eq. (7) λ_1(upward triangles), λ_2(downward triangles) and λ_3(circles) as functions of temperature. For the logarithmic representation, negative values of λ_2 and λ_3 are presented.

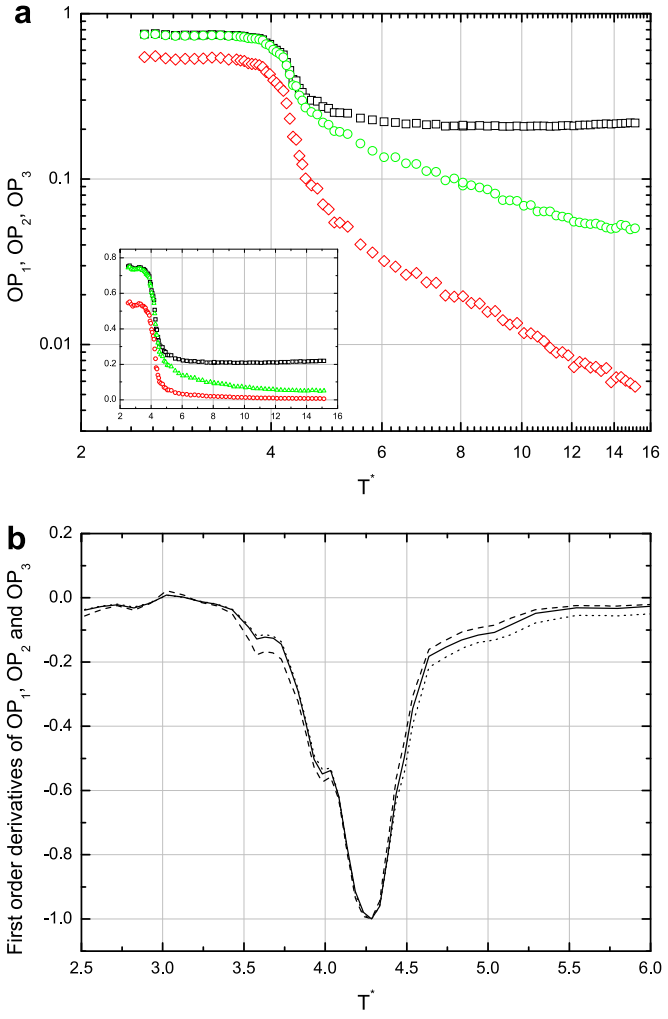

Fig. 9. (a) Comparison of the temperature dependencies of the different order parameter definitions, OP_1 (squares), OP_2 (diamonds), OP_3 (circles). The order parameters are presented both in double logarithmic scale and linear scale (the inset).(b) First order derivatives of the order parameters shown in plot (a). The minima of these curves appear at the same temperature $T^* \cong 4.23$.

3.3.2. Correlation between chain dimension and ordering of chain segments

The similar temperature dependency of the chain dimension $\langle Rg^{*2}\rangle$ and the order parameter at low temperatures implies that the change of the overall chain shape might be driven by the ordering of the stiff chain segments. In Fig. 10 we present the relationship between the radius of gyration and its principal components and the order in the chain molecule, using OP_2. In this representation the coil and globule states have practically zero-order parameter, only marginally varying with the shape of the molecule. We therefore observe a steep variation of the size parameters with the order, indicating that there is no correlation between *Rg* and the order parameter in the coiled and globular states.

However, as soon as we approach the transition temperature $T^* \cong 4.23$, the radius of gyration and its principle components vary linearly with the order in the chain. The linear dependence of *Rg* is dominated by the change with order of the largest principal moment of inertia. In contrast the two other principle moments of inertia decrease linearly with OP_2. Wang and Warner [80] derived a theoretical relationship for the end-to-end distance and its principal components as a function of the order parameter in an ideal freely jointed chain of (long) stiff segments. Moreover, adapting the usual relationship between the radius of gyration and end-to-end distance $\langle R^2\rangle$ valid for sufficiently linear ideal chains, viz. $\langle R_g^2\rangle = \frac{1}{6}\langle R^2\rangle$, they predicted the following relationships

$$\left\langle L_1^{*2}\right\rangle = \frac{1}{6}N\ell_0^{*2}\left\langle \cos^2(\theta)\right\rangle = \frac{1}{18}N\ell_0^{*2}(2OP_2+1) \tag{9a}$$

and

$$\left\langle L_2^{*2}\right\rangle = \left\langle L_3^{*2}\right\rangle \frac{1}{18}N\ell_0^{*2}(1-OP_2) \tag{9b}$$

with $\ell_0$the bond length of the freely jointed chain.

The interacting chain studied in this work seems to obey a similar linear relationship between the principle components of the radius of gyration and the order in the chain (see Fig. 10), with the provision that the proportionality constants in equation 9(a) and (b) differ from the theoretical constants derived for the ideal freely jointed chain.

Again, we should notice that different order parameters may give different results. For example, using OP_1 instead of OP_2, a positive slope of *Rg* versus OP_1 will be found in the uninteresting low order region of Fig. 10 (but with OP_1 now starting at a non-zero value of ca. $OP_1 \sim 0.2$). However, in the region of higher order the linear relationship between (the principal components of) the radius of gyration and the order parameter remains valid.

3.4. All-trans stems and chain folded lamellar crystal shape

3.4.1. All-trans stems

According to our definition of the *all-trans* segment, the number and the average length of *all-trans* segments are calculated and presented in Fig. 11 as a function of temperature. It is worth mentioning that the length of an *all-trans* stem is defined by the number of the contained chain units instead of the distance between the end units. From low temperature to high temperature, the average length of the *all-trans* segments decreases monotonically; we clearly see a two-stage behavior. At the low temperatures the average stem length drops very quickly with increasing temperature whereas at the high temperatures the average stem length slowly decays to a limiting value of 2, i.e. the high temperature limiting value. The steepest change of the stem length occurs, again, at the transition temperature $T^* \cong 4.23$. At the same time, starting at the low temperature, the total number of the all-trans segments increases drastically, reaching a maximum at $T^* \cong 4.54$

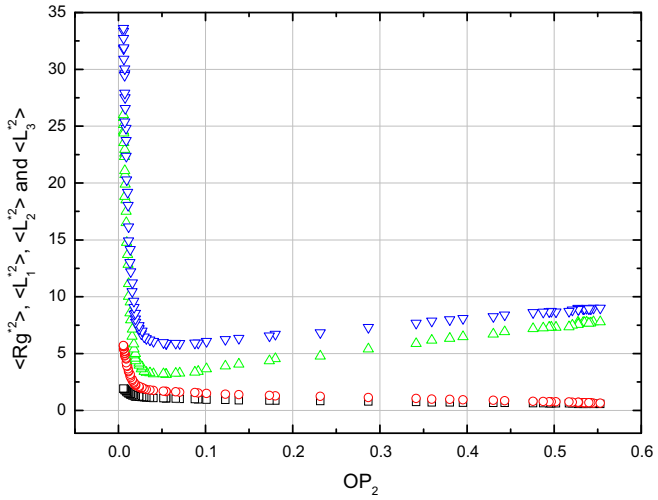

Fig. 10. Correlation between mean squared radius of gyration (downward triangles) and its principal components $\langle L_1^{*2}\rangle$ (upward triangles), $\langle L_2^{*2}\rangle$ (circles) and $\langle L_3^{*2}\rangle$ (squares) and the order parameter OP_2.

and then decreasing monotonically to high temperature. This is consistent with the picture of the long rigid segments breaking into smaller pieces, which cause the shortening in length and the increase in the number of the stretches of *all-trans* segments.

In all previous sections we have observed for the different properties considered the same transition temperature from the chain folded lamella-to-the globule. The most precise way to determine the transition temperature is from the first derivative with respect to temperature as explicitly shown for the order parameters OP_1, OP_2, and OP_3, in Fig. 9(b). For all other properties discussed here the first derivative always shows the most pronounced change at the transition temperature $T^* \cong 4.23$, clearly indicating the consistency as well as-we believe-the accuracy of our data.

3.4.2. Lamellar equilibrium thickness

We are now in a position to return to the size of the chain folded lamellar crystal as a function of temperature. It was already mentioned in the section on the radius of gyration and its principal components that our data clearly showed a decrease in the lamellar fold length (in terms of $\sqrt{\langle L_1^{*2}\rangle}$ of $\langle R_g^{*2}\rangle$) upon approaching the

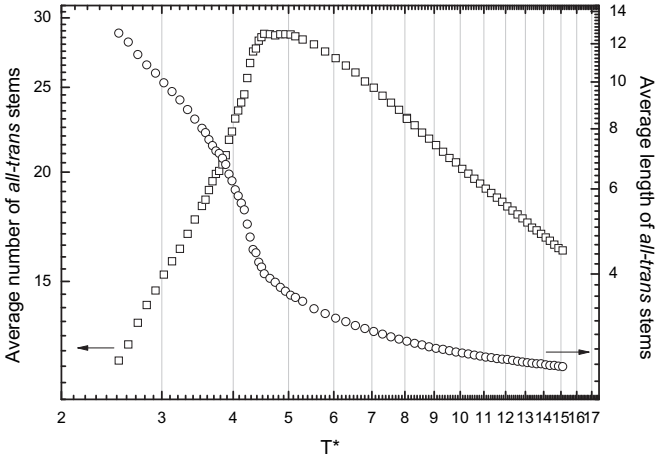

Fig. 11. The average number (squares) and average length (circles) of the *all-trans* stems as a function of temperature.

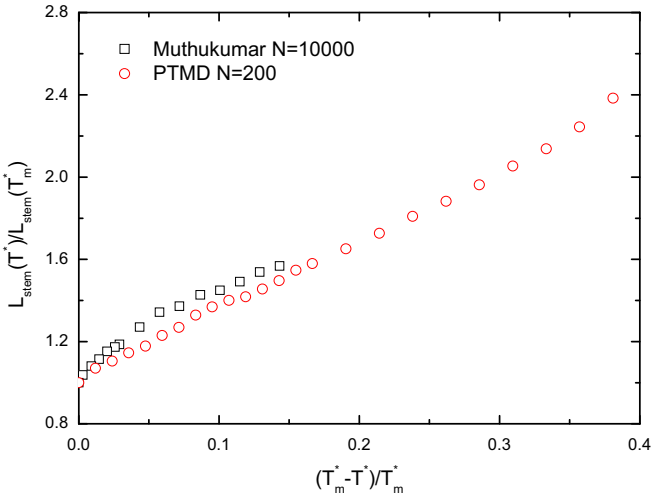

Fig. 12. Comparison of the relative average stem length obtained by Muthukumar's theory (squares) and our REMD simulation (circles) and as a function of super cooling.

transition temperature $T^* \cong 4.23$. This was in contrast with earlier simulations who discussed the increase of the lamellar thickness upon approaching the melting temperature in agreement with conventional crystallization/melting theory [47,72–74,81,82].

However, it is more appropriate to compare our simulation results for the single chain to a equilibrium theory for single chain crystallization recently presented by Muthukumar [83,84] and followed by Larini et al. [19]. Muthukumar derived an expression for the free energy of the chain folded crystal, including the entropy originating from the arrangement of the chain segments in the chain folds of the chain folded crystal. The equilibrium state of the chain folded crystal corresponds to a lamellar crystal of finite thickness mainly stabilized by the numerous ways to arrange the chain segments in the fold loops. According to Muthukumar the equilibrium thickness of the single chain crystal, defined by the stem length, decreases with decreasing super cooling, reaching a finite thickness at the equilibrium melting temperature of the chain folded crystal. In Fig. 12 we present the relative average stem length $(\langle L_{stem}(T^*)\rangle)/(\langle L_{stem}(T^*_m)\rangle)$ as a function of the relative super cooling $((\Delta T^*)/(T^*_m)) = ((T^*_m - T^*)/(T^*_m))$, with $T^* \cong 4.23$, the *chain folded lamellar crystal to globule* transition temperature determined

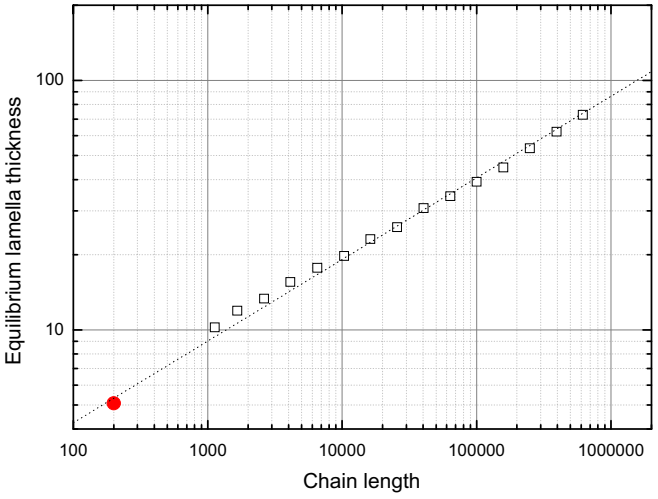

Fig. 13. The equilibrium lamella thickness at T^*_mcalculated by Muthukumar (squares) and from our REMD simulation data (circle). The dotted line is a fit of power function to guide the eye.

in our simulations. In this representation we can compare immediately with the data of Muthukumar [85].

Our simulation results are in semi-quantitative agreement with these theoretical predictions and are, as far as the authors are aware, the first quantitative simulation results that confirm these theoretical predictions, signifying that the theoretical approximations made by Muthukumar are capturing the essentials of single chain crystal melting. One could argue that our data are for a much shorter chain length as the data presented by Muthukumar, but the relative stem length versus relative super cooling representation hints even to the occurrence of universal behavior independent of chain length. Moreover, in Fig. 13 we compare the absolute value of the equilibrium thickness obtained in our simulation at the equilibrium transition temperature $T^* \cong 4.23$ with the data of Muthukumar for the equilibrium thickness at the equilibrium melting temperature obtained for much higher chain lengths. Clearly, our result seems to be in excellent agreement with the results of Muthukumar. We believe this demonstrates the accuracy of our simulation data and that the approach of Muthukumar captures the essence of the single chain folded crystals.

The observed increase in lamellar thickness with decreasing super cooling in the previous conventional MD studies are very likely a result of the chain being trapped in a local minimum of the rugged phase space landscape not being able to overcome the high energy barriers in the available simulation time. Therefore in a conventional MD simulation we may not expect to get correct ensemble averaged sampling.

4. Conclusion

In the present work, we have re-investigated the long-standing topic of the single chain and re-interpreted thermodynamic data against some recently developed theory. A polyethylene chain with $N = 200$ CH_2 units was simulated using replica exchange molecular dynamics. Simulations were performed in a broad temperature range covering both the coil-to-globule and the globule-to-chain folded crystal transition of the polymer chain and for intra-chain interactions varying from the fully interacting to the ideal spring chain. The REMD provided reliable simulation data on the equilibrium properties of the polymer chain at all temperatures, which is not easy to achieve in conventional MD or MC simulations as they get easily trapped in local minima separated by large energy barriers. This work demonstrates that REMD is a very efficient method to obtain equilibrium data.

In the analysis of the simulation data we focus on the thermodynamics, chain conformational properties and the transitions between the different conformational states.

Thermodynamic properties, including the potential energy density distributions, isothermal heat capacities, the absolute free energy, entropy and internal energy of the chain molecule are obtained and discussed. It is found that the coil-to-globule transition is dominated by the vdW energy, whereas the globule-to-folded chain transition is accompanied by transitional behavior in the torsional energy – creating long *all-trans* stems in the chain folded state- and in the vdW energy-attributed to non-bonded interactions between the segments in the aligned *all-trans* stems.

Our data clearly show that for the interaction potential model and chain length considered here, the chain folded crystal to globule transition is not a first order transition but is a continuous transition with smoothed steps in entropy and internal energy at the transition temperature. Nevertheless, from all studied chain properties we obtain the same value for the transition temperature, which allows us to establish with good accuracy the equilibrium transition temperature for the chain folded crystal to globule transition.

A set of orientational order parameters has been determined and was used to investigate the order in the polymer chain. At the globule-to-folded chain transition an abrupt change in the value of the order parameter is observed, whereas there is no or almost no change in the value of the order parameter at the coil-to-globule transition temperature. Some frequently used order parameters (OP_1, OP_3, λ_2, λ_3) also give at the highest temperatures (where we expect no order in the chain conformation) a non-zero value for the order parameter. The order parameter OP3 predicts in addition significant order also in the globular state whereas the other order parameters (OP_1, OP_2, λ_2, λ_3) only show a steep change in the order parameter going from the folded chain to the globule and expanded coil states. Only the order parameter OP_2 approaches asymptotically zero-order at high temperatures, which makes it most likely to be preferred to discuss the order in the chain conformation. The (apparent) order in the disordered globular and coiled states indicated by some of the studied order parameters is related to the definition of the order parameter and will depend on the chain length of the polymer.

The radius of gyration and its principal components show two transition temperatures for a PE chain with the lower transition temperature corresponding to the folded chain lamella to chain globule transition and the higher transition temperature corresponding to the globule-to-coil transition. The radius of gyration and its largest principal component decrease with increasing temperature. In earlier simulations the radius gyration and its largest principal component slightly increased or remained constant with temperature. This was interpreted to be in agreement with the results expected from classical crystallization theories.

In agreement with the temperature dependence found for the (largest principal component of the) radius of gyration, it is found that below the equilibrium melting temperature of the single chain crystal, the equilibrium lamellar thickness of the folded chain crystal decreases with increasing temperature, which is opposite to the prediction of classical crystallization theories but complies with the recent theories of Muthukumar [83] and Larini et al. [19]. The agreement between the simulations and the theoretical predictions are semi-quantitative and may even hint to universal behavior of the relative equilibrium chain folded crystal thickness and the relative super cooling. Our results give support to the theory of Muthukumar and the theoretical approximations made to predict the equilibrium properties of the chain folded crystal as a function of super cooling and chain length.

Acknowledgement

The authors thank the Funds for Scientific Research Flanders for financial support. L.T. is indebted to the Katholieke Universiteit Leuven for a postdoctoral fellowship (OT 03/93). The computations for this research have been done on the VIC HPC supercomputer of the K.U.Leuven.

Appendix A. Supplementary material

Supplementary data associated with this article can be found, in the online version, at doi:10.1016/j.polymer.2010.09.019.

References

[1] Xu J, Zhu Z, Luo S, Wu C, Liu S. First observation of two-stage collapsing kinetics of a single synthetic polymer chain. Physical Review Letters 2006;96:27802.
[2] Wang X, Wu C. Light-scattering study of coil-to-globule transition of a poly(N-isopropylacrylamide) chain in deuterated water. Macromolecules 1999;32:4299–301.
[3] Wang X, Qiu X, Wu C. Comparison of the coil-to-globule and the globule-to-coil transitions of a single poly(n-isopropylacrylamide) homopolymer chain in water. Macromolecules 1998;31:2972–6.
[4] Wu C, Zhou S. First observation of the molten globule state of a single homopolymer chain. Physical Review Letters 1996;77:3053.
[5] Chu B, Ying Q, Grosberg AY. Two-stage kinetics of single-chain collapse. Polystyrene in cyclohexane. Macromolecules 1995;28:180–9.
[6] Swislow G, Sun S, Nishio I, Tanaka T. Coil-globule phase transition in a single polystyrene chain in cyclohexane. Physical Review Letters 1980;44:796.
[7] Huser T, Yan M, Rothberg LJ. Single chain spectroscopy of conformational dependence of conjugated polymer photophysics. Proceedings of the National Academy of Sciences of the United States of America 2000;97:11187–91.
[8] Tanaka T. Phase transitions in gels and a single polymer. Polymer 1979;20:1404–12.
[9] Perkins T, Smith D, Chu S. Direct observation of tube-like motion of a single polymer chain. Science 1994;264:819–22.
[10] Deniz AA, Mukhopadhyay S, Lemke EA. Single-molecule biophysics: at the interface of biology, physics and chemistry. Journal of The Royal Society Interface 2008;5:15–45.
[11] Perkins T, Smith D, Larson R, Chu S. Stretching of a single tethered polymer in a uniform flow. Science 1995;268:83–7.
[12] Kumaki J, Nishikawa Y, Hashimoto T. Visualization of single-chain conformations of a synthetic polymer with atomic force microscopy. Journal of the American Chemical Society 1996;118:3321–2.
[13] Kumaki J, Hashimoto T. Conformational change in an isolated single synthetic polymer chain on a mica surface observed by atomic force microscopy. Journal of the American Chemical Society 2003;125:4907–17.
[14] Ortiz C, Hadziioannou G. Entropic elasticity of single polymer chains of poly(methacrylic acid) measured by atomic force microscopy. Macromolecules 1999;32:780–7.
[15] Bemis JE, Akhremitchev BB, Walker GC. Single polymer chain elongation by atomic force microscopy. Langmuir 1999;15:2799–805.
[16] Rief M, Oesterhelt F, Heymann B, Gaub HE. Single molecule force spectroscopy on polysaccharides by atomic force microscopy. Science 1997;275:1295–7.
[17] Zlatanova J, Lindsay S.M, Leuba S.H. Single molecule force spectroscopy in biology using the atomic force microscope. Progress in Biophysics and Molecular Biology;74:37–61.
[18] Fritz J, Anselmetti D, Jarchow J, Fernandez-Busquets X. Probing single biomolecules with atomic force microscopy. Journal of Structural Biology 1997;119:165–71.
[19] Larini L, Barbieri A, Prevosto D, Rolla PA, Leporini D. Equilibrated polyethylene single-molecule crystals: molecular-dynamics simulations and analytic model of the global minimum of the free-energy landscape. Journal of Physics Condensed Matter 2005;17:L199.
[20] Stockmayer WH. Problems of the statistical thermodynamics of dilute polymer solutions. Die Makromolekulare Chemie 1960;35:54–74.
[21] Mattice WL, Suter UW. Conformational theory of large molecules: the rotational isomeric state model in macromolecular systems. 1st ed. Wiley-Interscience; 1994.
[22] Flory PJ. Statistical mechanics of chain molecules, reprint. Oxford Univ Pr (Sd); 1989.
[23] Yamakawa H. Modern theory of polymer solutions. Harper & Row; 1971.
[24] Binder K, Paul W, Strauch T, Rampf F, Ivanov V, Luettmer-Strathmann J. Phase transitions of single polymer chains and of polymer solutions: insights from Monte Carlo simulations. Journal of Physics Condensed Matter 2008;20:494215.
[25] Liao Q, Jin X. Formation of segmental clusters during relaxation of a fully extended polyethylene chain at 300 K: a molecular dynamics simulation. The Journal of Chemical Physics 1999;110:8835.
[26] Baumgärtner A. Statics and dynamics of the freely jointed polymer chain with Lennard-Jones interaction. The Journal of Chemical Physics 1980;72:871.
[27] Jeppesen C, Kremer K. Single-chain collapse as a first-order transition: model for PEO in water. Europhysics Letters 1996;34:563–8.
[28] Hu W. Structural transformation in the collapse transition of the single flexible homopolymer model. The Journal of Chemical Physics 1998;109:3686.
[29] Wittkop M, Kreitmeier S, Göritz D. The collapse transition of a single polymer chain in two and three dimensions: a Monte carlo study. The Journal of Chemical Physics 1996;104:3373.
[30] Noguchi H, Yoshikawa K. Morphological variation in a collapsed single homopolymer chain. The Journal of Chemical Physics 1998;109:5070.
[31] Taylor MP, Paul W, Binder K. Phase transitions of a single polymer chain: a Wang–Landau simulation study. The Journal of Chemical Physics 2009;131:114907.
[32] Narambuena C, Leiva E, Chávez-Páez M, Pérez E. Effect of chain stiffness on the morphology of polyelectrolyte complexes. A Monte Carlo simulation study. Polymer 2010;51:3293–302.
[33] Ivanov VA, Stukan MR, Müller M, Paul W, Binder K. Phase diagram of solutions of stiff-chain macromolecules: a monte carlo simulation. The Journal of Chemical Physics 2003;118:10333.
[34] Stukan MR, Ivanov VA, Grosberg AY, Paul W, Binder K. Chain length dependence of the state diagram of a single stiff-chain macromolecule: theory and monte carlo simulation. The Journal of Chemical Physics 2003;118:3392.
[35] Kremer K, Binder K. Monte carlo simulation of lattice models for macromolecules. Computer Physics Reports 1988;7:259–310.
[36] Zhou Y, Hall CK, Karplus M. First-order disorder-to-order transition in an isolated homopolymer model. Physical Review Letters 1996;77:2822–5.

[37] Liang H, Chen H. First-order transition of a homopolymer chain with Lennard-Jones potential. The Journal of Chemical Physics 2000;113:4469.
[38] Baysal BM, Karasz FE. Coil-globule collapse in flexible macromolecules. Macromolecular Theory and Simulations 2003;12:627–46.
[39] Takahashi M, Yoshikawa K, Vasilevskaya VV, Khokhlov AR. Discrete coil? globule transition of single duplex DNAs induced by polyamines. The Journal of Physical Chemistry B 1997;101:9396–401.
[40] Swislow G, Sun S, Nishio I, Tanaka T. Coil-globule phase transition in a single polystyrene chain in cyclohexane. Physical Review Letters 1980;44:796–8.
[41] Martemyanova JA, Stukan MR, Ivanov VA, Müller M, Paul W, Binder K. Dense orientationally ordered states of a single semiflexible macromolecule: an expanded ensemble Monte Carlo simulation. The Journal of Chemical Physics 2005;122:174907.
[42] Liao Q, Dobrynin AV, Rubinstein M. Counterion-correlation-induced attraction and necklace formation in polyelectrolyte solutions: theory and simulations. Macromolecules 2006;39:1920–38.
[43] Berghmans H, Deberdt F. Phase behaviour and structure formation in solutions of vinyl polymers. Royal Society of London Philosophical Transactions Series A 1994;348:117–28.
[44] Rampf F, Binder K, Paul W. The phase diagram of a single polymer chain: new insights from a new simulation method. Journal of Polymer Science Part B Polymer Physics 2006;44:2542–55.
[45] Doye JPK, Sear RP, Frenkel D. The effect of chain stiffness on the phase behaviour of isolated homopolymers. Journal of Chemical Physics 1998;108:2134–42.
[46] Chen CM, Higgs PG. Monte-Carlo simulations of polymer crystallization in dilute solution. Journal of Chemical Physics 1998;108:4305–14.
[47] Iwata M, Sato H. Chain movement in crystallization process by molecular dynamics simulation. Physical Chemistry Chemical Physics 1999;1:2491–500.
[48] Swendsen RH, Wang JS. Replica Monte Carlo simulation of spin-glasses. Physical Review Letters 1986;57:2607–9.
[49] Geyer C,J, Keramidas E.M. In computing science and statistics: Proceedings of the 23rd symposium on the interface. Keramidas EM, editor. (n.d.). p. 156–63.
[50] Sugita Y, Kitao A, Okamoto Y. Multidimensional replica-exchange method for free-energy calculations. The Journal of Chemical Physics 2000;113:6042.
[51] Wang J.S, Swendsen R.H. Replica monte carlo simulation (revisited), progress of theoretical physics-supplement; 2005. p. 317–23.
[52] Berg BA, Neuhaus T. Multicanonical algorithms for first order phase transitions. Physics Letters B 1991;267:249–53.
[53] Berg Neuhaus. Multicanonical ensemble: a new approach to simulate first-order phase transitions. Physical Review Letters 1992;68:9–12.
[54] Berg BA, Celik T. New approach to spin-glass simulations. Physical Review Letters 1992;69:2292.
[55] Paul W, Müller M. Enhanced sampling in simulations of dense systems: the phase behavior of collapsed polymer globules. The Journal of Chemical Physics 2001;115:630.
[56] Paul W, Müller M. Enhanced sampling in simulations of dense systems. Computer Physics Communications 2002;146:113–7.
[57] Swendsen RH, Wang J. Replica monte carlo simulation of spin-glasses. Physical Review Letters 1986;57:2607.
[58] Sugita Y, Okamoto Y. Replica-exchange molecular dynamics method for protein folding. Chemical Physics Letters 1999;314:141–51.
[59] Earl DJ, Deem MW. Parallel tempering: theory, applications, and new perspectives. Physical Chemistry Chemical Physics 2005;7:3910–6.
[60] Muthukumar M. Modeling polymer crystallization. In: Interphases and Mesophases in Polymer Crystallization III; 2005. p. 241–74.
[61] Ryckaert JP, Bellemans A. Molecular dynamics of liquid alkanes. Faraday Discussions of the Chemical Society 1978;66:95–106.
[62] Sundararajan PR, Kavassalis TA. Molecular dynamics study of polyethylene chain folding: the effects of chain length and the torsional barrier, Journal of the Chemical Society. Faraday Transactions 1995;91:2541–9.
[63] Mayo SL, Olafson BD, Goddard WA. DREIDING: a generic force field for molecular simulations. Journal of Physical Chemistry 1990;94:8897–909.
[64] Tobias DJ, Martyna GJ, Klein ML. Molecular dynamics simulations of a protein in the canonical ensemble. The Journal of Physical Chemistry 1993;97:12959–66.
[65] Zhou Y, Karplus M, Wichert JM, Hall CK. Equilibrium thermodynamics of homopolymers and clusters: molecular dynamics and Monte Carlo simulations of systems with square-well interactions. The Journal of Chemical Physics 1997;107:10691.
[66] Vettorel T, Meyer H, Baschnagel J, Fuchs M. Structural properties of crystallizable polymer melts: intrachain and interchain correlation functions. Physical Review E Stat Nonlin Soft Matter Physics 2007;75:041801.
[67] Vettorel T. Ph.D. thesis. URL. Université Louis Pasteur Strasbourg, http://eprints-scd-ulp.u-strasbg.fr:8080/334/01/THESE_T_VETTOREL.PDF; 2005.
[68] Meyer H. Aspects of polymer crystallization: molecular dynamics simulations with atomistic and coarse-grained models. URL, https://www.ornl.gov/cnms/nanofocul2006/pdfs/meyer.pdf; 2006.
[69] Šolc K. Shape of a random flight chain. The Journal of Chemical Physics 1971;55:335.
[70] Rubinstein M, Colby RH. Polymer physics. USA: Oxford University Press; 2003.
[71] Kavassalis TA, Sundararajan PR. A molecular-dynamics study of polyethylene crystallization. Macromolecules 1993;26:4144–50.
[72] Fujiwara S, Sato T. Structure formation of a single polymer chain. I. Growth of trans domains. The Journal of Chemical Physics 2001;114:6455.
[73] Liu C, Muthukumar M. Langevin dynamics simulations of early-stage polymer nucleation and crystallization. The Journal of Chemical Physics 1998;109:2536.
[74] Zhang X, Li Z, Lu Z, Sun CC. The reorganization of the lamellar structure of a single polyethylene chain during heating: molecular dynamics simulation. The Journal of Chemical Physics 2001;115:10001.
[75] Fujiwara S, Sato T. Molecular dynamics simulation of structural formation of Short polymer chains. Physical Review Letters 1998;80:991–4.
[76] Wilson M. Determination of order parameters in realistic atom-based models of liquid crystal systems. Journal of Molecular Liquids 1996;68:23–31.
[77] Eppenga R, Frenkel D, Laboratorium F, Utrecht R. Monte Carlo study of the isotropic and nematic phases of infinitely thin hard platelets. Molecular Physics 1984;52:1303–34.
[78] Fujiwara S, Sato T. Molecular dynamics simulations of structural formation of a single polymer chain: bond-orientational order and conformational defects. The Journal of Chemical Physics 1997;107:613.
[79] Saupe A. Recent results in the field of liquid crystals. Angewandte Chemie Int Ed Engl 1968;7:97–112.
[80] Wang XJ, Warner M. Theory of main chain nematic polymers with spacers of varying degree of flexibility. Liquid Crystals 1992;12:385–401.
[81] Doye JPK. Computer simulations of the mechanism of thickness selection in polymer crystals. Polymer 2000;41:8857–67.
[82] Toma L, Toma S, Subirana JA. Simulation of polymer crystallization through a dynamic monte carlo lattice model. Macromolecules 1998;31:2328–34.
[83] Muthukumar M, Shifting paradigms in polymer crystallization. In: Progress in understanding of polymer crystallization; 2007. p. 1–18.
[84] Muthukumar M. Molecular modelling of nucleation in polymers. Philosophical Transactions of the Royal Society of London. Series A Mathematical, Physical and Engineering Sciences 2003;361:539–56.
[85] The data of Muthukumar on equilibrium thickness versus super cooling and equilibrium thickness as a function of chain were obtained by digitizing the data points in Figures 1.9 and 1.10 in [83].